

Critical current density in Ag/YBa₂Cu₃O_x and PrBa₂Cu₃O_y/YBa₂Cu₃O_x multilayers

V. S. Dang^{1,*}, P. Mikheenko¹, A. Sarkar¹, J. S. Abell¹ and A. Crisan^{1,2}

¹School of Metallurgy and Materials, University of Birmingham, Birmingham B15-2TT, United Kingdom.

²National Institute of Materials Physics, Bucharest 077125, Romania

* Corresponding author e-mail: v.dang@bham.ac.uk

Abstract. One of successful methods of introducing artificial pinning centres in superconducting films is by alternating layers of superconducting material and incomplete layers (planar distributions of nanodots) of other materials (quasi-superlattice or quasi-multilayer approach). Most of the work on artificial pinning centres has been done on thin YBa₂Cu₃O_x (YBCO) films and a large variety of quasi-multilayer materials have been explored. It is still difficult to justify the choice of a quasi-multilayer material for particular superconducting applications. One of the properties to be taken into account is compatibility of the crystal lattice of YBCO and the quasi-superlattice material. Here we compare the superconducting behaviour of two very different quasi-multilayers: one with very similar crystal lattices of nanodots and YBCO: PrBa₂Cu₃O_y (PBCO)/YBCO, and another one with very different, Ag/YBCO. We found that the difference between crystal lattices strongly affects superconducting properties of quasi-multilayers and leads to different types of pinning in the films.

1. Introduction

There is an extensive literature on artificial pinning in YBa₂Cu₃O_x (YBCO) films. A few methods proved to be effective in increasing critical current density (J_c) in the films, at least for some materials and conditions of deposition. Among these methods are substrate decoration [1], quasi-multilayer approach [2] and distribution of secondary phase from a composite target [3]. Many materials have been used to introduce artificial pinning centres, for example, Y₂BaCuO₅ [2], Y₂O₃ [4, 5], yttrium stabilized zirconium (YSZ) [6], BaTMO₃ (TM = transition metal = Ir, Ti, Zr, Hf) [7], transition metals [8], Ag, Au, Pd and non-superconducting YBCO [9, 10]. Most of these materials were identified by trial and error approach and conditions of their use for particular applications are far from clear.

It is known that pure YBCO films grown by pulsed laser deposition (PLD) have a maximum in the J_c versus thickness (d) dependence at d_{max} between 50 and 400 nm, depending on the growth conditions [11]. For $d > d_{max}$, J_c strongly decreases with d . Most of the work is done world-wide on the films of the thickness close to d_{max} . There are, however a few exceptions, among them the work of ref. [12] and references therein. The research on thick films is especially important for applications.

Here we analyse how the difference in crystal lattices of YBCO and the quasi-multilayer material affects critical current in thick films following the example of two quasi-multilayers with similar

(PrBa₂Cu₃O_y (PBCO)/YBCO) and very different (Ag/YBCO) crystal lattices. YBCO and PBCO have a perovskite orthorhombic structure with close lattice parameters. The lattice parameters of YBCO are $a = 0.38178$ nm, $b = 0.38839$ nm and $c = 1.16828$ nm [13], while, for example, lattice parameters of superconducting PBCO are $a = 0.3875$ nm, $b = 0.3938$ nm and $c = 1.1808$ nm [14]. In contrast, Ag forms a simple face-centred cubic crystal lattice with crystal lattice parameter of 0.409 nm [15]. The quasi-multilayers under investigation are of a similar thickness and their properties are compared with a pure YBCO film of the same thickness of about 3 μm . The results show that differences in crystal lattices have strong implication on the character of pinning and affect the critical current (I_c) per centimetre of width, an important technological superconducting parameter of the films.

We have recently studied the increase in J_c in Ag/YBCO multilayers [9] of different architecture and found that Ag/YBCO multilayer composed of two 1.5- μm layers of YBCO with 15 laser pulses of Ag in-between, gives the highest J_c in a wide range of magnetic fields. Similar to that, PBCO/YBCO multilayer [16] with three 0.9- μm layers of YBCO separated by 2.4 nm of PBCO also gives the highest J_c , albeit in high fields above 2.5 T only. Our choice of thickness of about 3 μm is based on the experiments above.

2. Experiment

Ag and PBCO nano-dots and YBCO layers were grown on (100) SrTiO₃ (STO) substrates using an excimer KrF 248 nm laser with pulse duration of 30 ns, repetition rate of 4 Hz, laser energy density of 1.2 J/cm², laser energy inside the PLD chamber of about 130 mJ, and target–substrate distance of 5.5 cm, the laser having a scanning beam. In the scanning mode, the target material is gradually consumed without a need for frequent polishing of the target. This makes this technique potentially suitable for large-scale production of superconducting coated conductors.

The PBCO quasi-multilayer was composed of three PBCO quasi-layers (15 laser pulses each) and three layers of YBCO of the thickness of about 900 nm. All layers were grown at 781 °C in 50 Pa oxygen partial pressure. The total thickness of the sample was 2.7 μm . In Ag/YBCO quasi-multilayer, two quasi-layers of Ag were grown at 450 °C by 15 laser pulses in vacuum of 6×10^{-3} Pa and two layers of YBCO, each 1500 nm thick, were grown at the same conditions as YBCO in the first sample. The total thickness of Ag/YBCO quasi-multilayer was 3.0 μm . After the deposition, films were cooled to room temperature in a partial oxygen atmosphere of 6×10^4 Pa at a rate of 8 °C/min. A pure YBCO reference film having a thickness of 2.9 μm was grown at the same conditions as YBCO in quasi-multilayers. The thickness was measured by a cross-sectional optical and electron microscopy.

We investigated the surface topography of the nanodots on the substrate by atomic force microscopy (AFM) using high resolution AFM probes with diameter of curvature of 1-10 nm. The AFM images were analysed by WSxM 5.0 software [17]. Critical current density of the films was determined from DC magnetization loops measured on a *Quantum Design* Magnetic Properties Measurement System MPMS-XL, in DC field $\mu_0 H$ up to 4 T. To investigate anisotropy in the films, we have performed angle-dependent transport measurements on a 550 μm long and 45 μm wide micro-bridges that were produced by photolithography and chemical etching. Scanning and transmission electron microscopy (SEM, TEM) and energy dispersive x-ray analysis (EDX) were used to analyse element content, micro and nano structure of the samples.

3. Results and discussion

Figures 1 and 2 show AFM images of Ag and PBCO quasi-layers, respectively, deposited on STO single crystal substrates and grown at the temperature of 450 °C in vacuum with 15 laser pulses. It can be seen that the two quasi-layer architectures are quite different. Ag nanodots are distributed rather uniformly, with average diameter of about 11 nm, average height of 3 nm (figure 1) and some empty spaces between them. The PBCO nanodots (figure 2) cover the substrate almost entirely. Their diameter varies from a few nm up to 20-30 nm. The height of PBCO nanodots also strongly varies with an average value of 2.65 nm.

Critical current density J_c was calculated for these films from the DC magnetization loops using the equation:

$$J_c = \frac{4m}{a^2bd(1 - \frac{a}{3b})}, \quad (1)$$

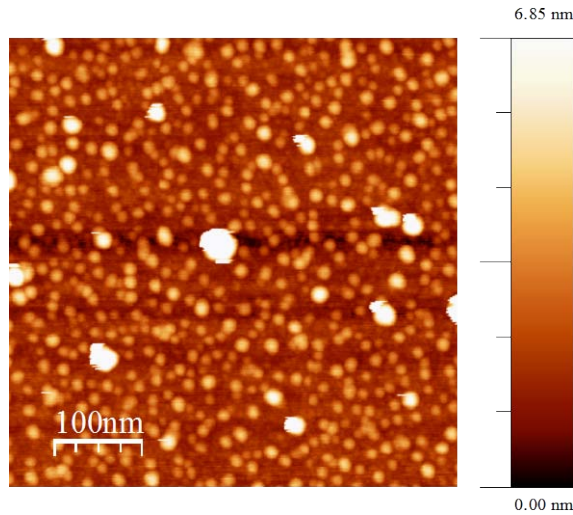


Figure 1. AFM image of Ag nanodots on STO substrate deposited at temperature of 450 °C in vacuum with 15 laser pulses.

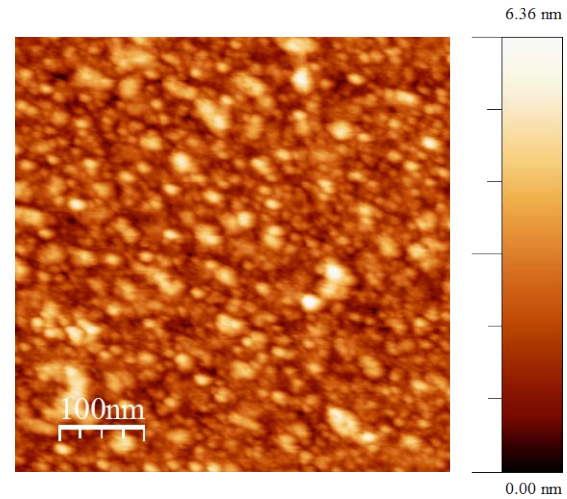


Figure 2. AFM image of PBCO nanodots on STO substrate deposited at temperature of 450 °C in vacuum with 15 laser pulses.

which is derived in SI units from a critical state model applied to thin films. In Eq. (1), m is the irreversible magnetic moment, or the half-width of the magnetisation loop, a and b ($a \leq b$) are the planar dimensions of the film, and d is the thickness. The equation (1) is not applicable below a characteristic magnetic field H_c [18], which is a function of J_c in our films at 77.3 K $\mu_0 H_c$ does not exceed 0.1 T. In magnetic field below H_c , J_c was determined by an exponential approximation from J_c at higher fields.

Because of the decrease of J_c with thickness above d_{max} , I_c in thick (few micrometers) YBCO samples is not very high. By using artificial pinning centres, we have achieved a shift of d_{max} toward a larger thickness [9]. The effect of such a shift is an increase in both J_c and I_c as is seen in figures 3 and 4.

Figure 3 shows field dependence of J_c at 77.3 K for Ag/YBCO and PBCO/YBCO quasi-multilayers in comparison with J_c of a pure YBCO film. It can be seen that J_c of Ag/YBCO quasi-multilayer is higher than J_c of the pure YBCO film at all fields in spite of the thickness of the latter being slightly smaller than the thickness of quasi-multilayer. The comparison is acceptable here because generally J_c decreases with film thickness. In PBCO/YBCO quasi-multilayer, the increase in J_c occurs in field above 2.5 T only. Figure 4 shows I_c for all samples as in Fig. 3. It can be seen that similar to J_c , I_c (the actual important parameter) in Ag/YBCO is higher than I_c in pure YBCO at all fields. In self-field, I_c of Ag/YBCO quasi-multilayer is about 1100 A/cm, almost 3 times higher than I_c of the pure YBCO film.

The nature of pinning centres created by Ag and PBCO quasi-layers can be clarified by scaling the angle dependence of critical current density $J_c(\theta, H)$. One of the approaches uses direct Blatter's et al. scaling related to the effective mass of charge carriers [19]. It was first applied to coated conductors by Civale et al. [20]. In this approach, the correlated and uncorrelated pinning centres can be identified from a plot of J_c versus effective magnetic field $H_{eff} = \varepsilon(\theta)H$, where $\varepsilon^2(\theta) = \cos^2\theta + \gamma^{-2}\sin^2\theta$, γ is the

anisotropy factor and θ is the angle between the magnetic field and c -axis of YBCO. Figure 5 and 7 show typical $J_c(\theta, H)$ curves at 77.3 K for different fields from 3 to 6 T in Ag/YBCO and PBCO/YBCO quasi-multilayers, respectively. When the magnetic field is applied in the direction close to the c -axis, a weak peak is observed in $J_c(\theta)$ in both quasi-multilayers. This peak is attributed to correlated extended defects created by Ag and PBCO nanodots.

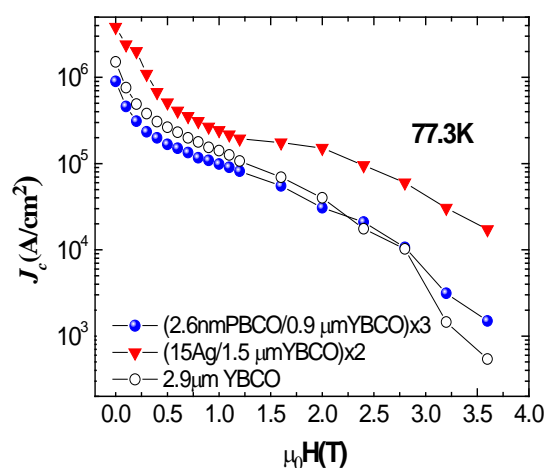


Figure 3. $J_c(H)$ dependence in Ag/YBCO quasi-multilayer with the total thickness of 3 μm , PBCO/YBCO quasi-multilayer of the thickness of 2.7 μm and reference pure 2.9- μm YBCO film. The legend indicating samples is shown in the plot.

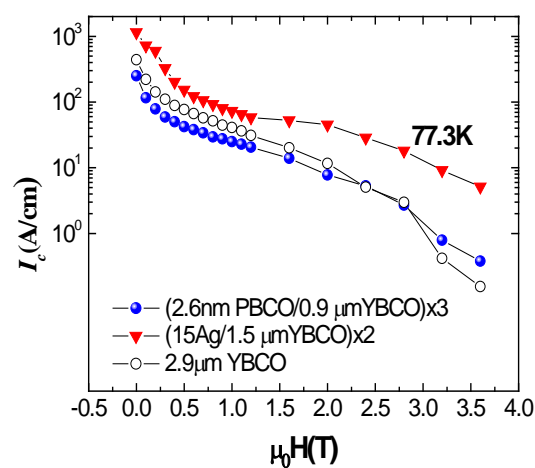


Figure 4. Total critical current per centimetre of width as function of magnetic field $I_c(H)$ for the same samples as in Fig 3.

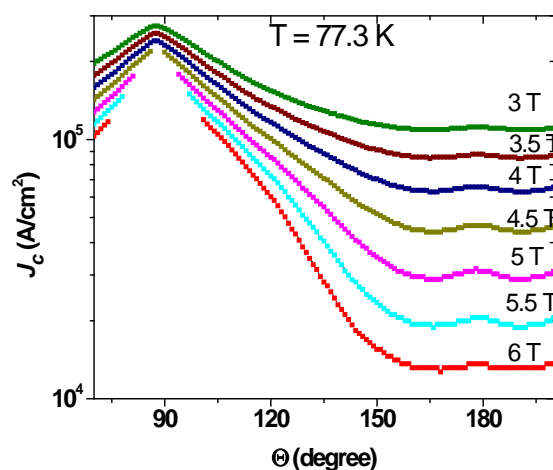


Figure 5. Angular dependence of critical current density in Ag/YBCO quasi-multilayer at different magnetic fields from 3 to 6 T at temperature of 77.3 K

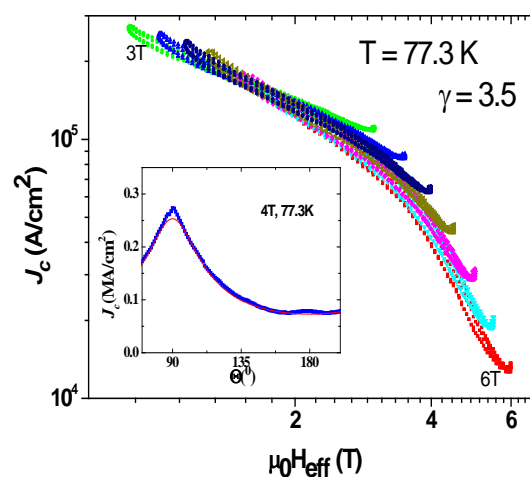


Figure 6. Best scaling of $J_c(\theta, H)$ at 77.3 K assuming $\gamma = 3.5$ in Ag/YBCO multilayer. Inset: total value of $J_c(\theta)$ at 77.3 K and 4 T (blue points) and the uncorrelated defects contribution (red line).

Figures 6 and 8 show the effective field scaling for Ag/YBCO (Fig 6) and PBCO/YBCO (Fig 8) quasi-multilayers at 77.3 K. The best scaling was achieved with $\gamma = 3.5$ for Ag/YBCO and a smaller $\gamma = 2.5$ for PBCO/YBCO. The anisotropy in quasi-multilayers is quite low comparable with $\gamma \sim 5-7$ obtained in standard TFA-YBCO films [21]. The correlated defects contribution can be determined from the plots such as those in insets of figures 6 and 8. In Ag/YBCO, a very weak contribution is detected for $H \parallel c$ ($\Theta = 180^\circ$) and it is even smaller in PBCO/YBCO, whereas a strong correlated contribution is seen for $H \parallel ab$ in PBCO/YBCO.

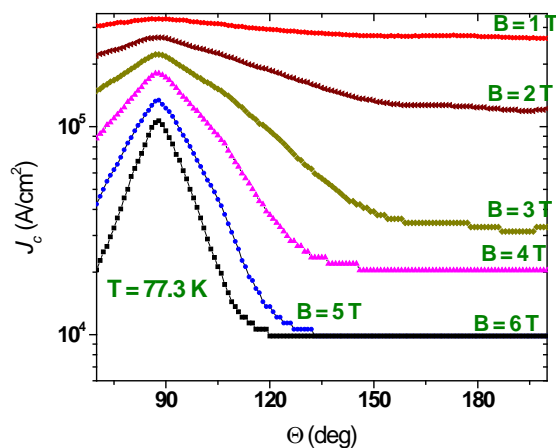


Figure 7. Angular dependence of critical current density in PBCO/YBCO quasi-multilayer at different magnetic fields from 1 to 6 T at temperature of 77.3 K

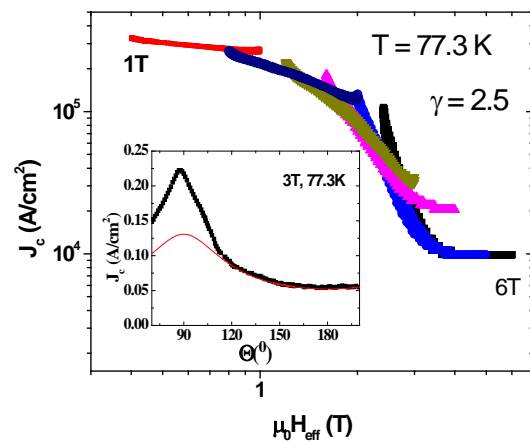


Figure 8. Best scaling of $J_c(\theta, H)$ at 77.3K assuming $\gamma = 2.5$ in PBCO/YBCO quasi-multilayer. Inset: total value of $J_c(\theta)$ at 77.3 K and 3 T (black points) and the uncorrelated defects contribution (red line).

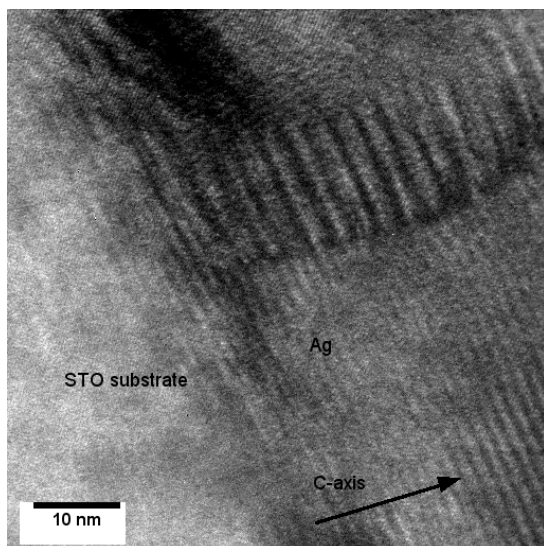


Figure 9. TEM image of Ag/YBCO quasi-multilayer taken at the interface with STO substrate.

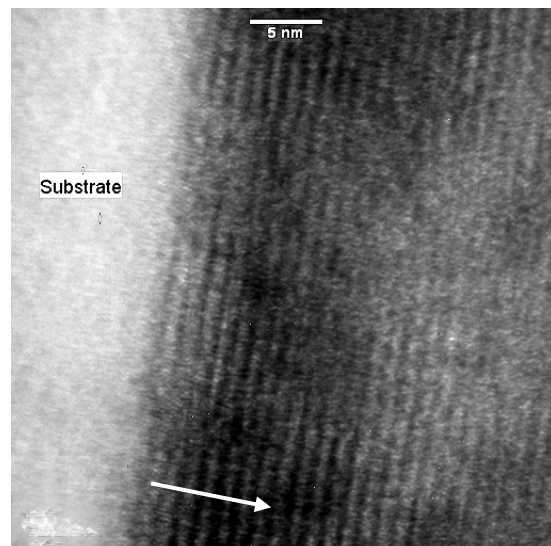


Figure 10. TEM image of PBCO/YBCO quasi-multilayer taken at the interface with STO.

The nanostructure of quasi-multilayers has been investigated in the vicinity of the interface with the STO substrate by TEM. The corresponding images for Ag/YBCO and PBCO/YBCO are shown in figures 9 and 10. The cross-sectional TEM images were obtained using bright-field conditions and are viewed along the $\langle 100 \rangle$ direction of YBCO. For Ag/YBCO quasi-multilayer (Fig. 9), the presence of an Ag particle with diameter around 12 nm has been detected and a c -axis extended defect is clearly visible. In PBCO/YBCO quasi-multilayer (figure 10) it is difficult to see the presence of PBCO due to its very close lattice structure to YBCO.

Due to the similar lattices of PBCO and YBCO, one would not expect very strong c -axis extended defects, but a good epitaxy would enhance J_c along the ab -plane, as seen in the inset to figure 8. In contrast, Ag nano-dots are able to create strong extended defects due to the mismatch between STO and YBCO. This produces clear peaks at $\Theta = 180^\circ$ in figures 5 and 6.

In conclusion, we found an increase of J_c along the c -axis of YBCO in both Ag/YBCO and PBCO/YBCO quasi-multilayers; the Ag/YBCO shows a significant increase in J_c in both high and low magnetic fields, while the PBCO/YBCO quasi-multilayer shows increase in high magnetic field only. The reason of such a different behaviour is in the compatibility of crystal lattices in nanodots and YBCO. The large difference between crystal lattice parameters promotes c -axis pinning, while small difference increases ab -plane correlated pinning and insures high ab -plane critical current in high magnetic field. By increasing the thickness, the self-field total current in Ag/YBCO quasi-multilayer as high as 1100 A/cm has been achieved. The angle-dependent transport measurements and TEM images support the evidence of correlated pinning in PBCO/YBCO and Ag/YBCO quasi-multilayers.

4. Acknowledgements

The financial support of the European Commission through the Marie Curie Excellence Grant MEXT-CT-2006-041111 "NanoTechPinningHTS", the ESF-NES Network, and the Romanian Ministry of Education and Research, is gratefully acknowledged.

References

- [1] Crisan A, Fujiwara S, Nie J C, Sundaresan A, Ihara H 2001 *Appl. Phys. Lett.* **79** 4547
- [2] Haugan T, Barnes P N, Wheeler R, Mwisenkothen F and Sumption M 2004 *Nature* **430** 867
- [3] MacMannus-Driscoll J L, Foltyn S R, Jia Q X, Wang H, Serquis A, Civale L, Maiorov B, Hawley M E, Maley M P and Peterson D E 2004 *Nat. Mater.* **3** 439
- [4] Barnes P N, Haugan T J, Varanasi C V and Campbell T A 2004 *Appl. Phys. Lett.* **85** 4088
- [5] Cai C, Hänisch J, Hühne R, Stehr V, Mickel C, Gemming T and Holzapfel B 2005 *J. Appl. Phys.* **98** 123906
- [6] Cai C B, Zhang J C, Cao S X, C, Hänisch J, Hühne R and Holzapfel B 2007 *Physica C* **460-462** 1355
- [7] Backen E, Hänisch J, Hühne R, Tschardtke K, Engel S, Thersleff T, Schultz L and Holzapfel B 2007 *IEEE Trans. Appl. Supercond.*, **17** 3733
- [8] Hänisch J, Cai C, Stehr V, Hühne R, Lyubina J, Nenkov K, Fuchs G, Schultz L and Holzapfel B 2006 *Supercond. Sci. Technol.* **19** 534
- [9] Mikheenko P, Sarkar A, Dang V S, Tanner J L, Awang Kechik M M, Abell J S, and Crisan A 2009 *IEEE Trans. Appl. Supercond* **19** 3491
- [10] Sarkar A, Mikheenko P, Dang V S, Abell J S, and Crisan A 2009 *Physica C* **469** 1550
- [11] Pan A V, Pysarenko S, Dou S X 2006 *J. Appl. Phys.* **88** 232506
- [12] Foltyn S R, Civale L, Macmanus-Driscoll J L, Jia Q X, Maiorov B, Wang H and Maley M, 2007 *Nat Mater* **6** 631
- [13] Chaplot S L, Reichardt W, Pintschovius L, Pyka N 1992 *Journal of Physics and Chemistry of Solids* **53** 761
- [14] Ye J, Sadewasser S, Schilling J S, Zou Z, Matsushita A, Matsumoto T 1999 *Physica C* **328** 111

- [15] Kittel C 1986 *Introduction to solid state physics* New York : Wiley pp.646
- [16] Crisan A, Dang V S, Mikheenko P, Sarkar A, Tse Y Y, Bowen J, Abell JS 2010 *Physica C* **470** 55
- [17] Horcas I, Fernandez R, Gomez-Rodriguez J M, Colchero J, Gomez-Herrero J and Baro A M 2007 *Rev Sci Instrum* **78** 013705
- [18] Shantsev D V, Galperin Y M, and Johansen T H 2000 *Phys. Rev. B* **61** 9699
- [19] Blatter G, Geshkenbein V B, Larkin AI 1992 *Phys. Rev. Lett.* **68** 875
- [20] Civale L, Maiorov B, Serquis A, Willis J O, Coulter J Y, Wang H, Jia Q X, Arendt P N, Jaime M, MacManus-Driscoll J L, Maley M P, and Foltyn S R 2004 *J. Low Temp Phys.* **135** 87
- [21] Puig T and Obradors X 2000 *Phys Rev Lett* **84** 1571